Biogeosciences

An ensemble approach to simulate CO_2 emissions from natural fires

A. V. Eliseev[1,2], I. I. Mokhov[1,3,4], and A. V. Chernokulsky[1]

[1]A. M. Obukhov Institute of Atmospheric Physics RAS, Moscow, Russia
[2]Kazan Federal University, Kazan, Russia
[3]M. V. Lomonosov Moscow State University, Moscow, Russia
[4]Moscow Institute of Physics and Technology, Moscow, Russia

Correspondence to: A. V. Eliseev (eliseev@ifaran.ru)

Abstract. This paper presents ensemble simulations with the global climate model developed at the A. M. Obukhov Institute of Atmospheric Physics, Russian Academy of Sciences (IAP RAS CM). These simulations are forced by historical reconstructions of concentrations of well-mixed greenhouse gases (CO_2, CH_4, and N_2O), sulfate aerosols (both in the troposphere and stratosphere), extent of crops and pastures, and total solar irradiance for AD 850–2005 (hereafter all years are taken as being AD) and by the Representative Concentration Pathway (RCP) scenarios for the same forcing agents until the year 2300. Our model implements Glob-FIRM (Global FIRe Model) as a scheme for calculating characteristics of natural fires. Comparing to the original Glob-FIRM model, in our implementation, the scheme is extended by a module accounting for CO_2 release from soil during fires. The novel approach of our paper is to simulate natural fires in an ensemble fashion. Different ensemble members in the present paper are constructed by varying the values of parameters of the natural fires module. These members are constrained by the GFED-3.1 data set for the burnt area and CO_2 release from fires and further subjected to Bayesian averaging. Our simulations are the first coupled model assessment of future changes in gross characteristics of natural fires. In our model, the present-day (1998–2011) global area burnt due to natural fires is $(2.1 \pm 0.4) \times 10^6 \, \mathrm{km}^2 \, \mathrm{yr}^{-1}$ (ensemble mean and intra-ensemble standard deviation are presented), and the respective CO_2 emissions to the atmosphere are $(1.4 \pm 0.2) \, \mathrm{Pg \, C \, yr}^{-1}$. The latter value is in agreement with the corresponding GFED estimates. The area burnt by natural fires is generally larger than the GFED estimates except in boreal Eurasia, where it is realistic, and in Australia, where it is smaller than these estimates. Regionally, the mod-

elled CO_2 emissions are larger (smaller) than the GFED estimates in Europe (in the tropics and north-eastern Eurasia). From 1998–2011 to 2091–2100, the ensemble mean global burnt area is increased by 13 % (28 %, 36 %, 51 %) under scenario RCP 2.6 (RCP 4.5, RCP 6.0, RCP 8.5). The corresponding global emissions increase is 14 % (29 %, 37 %, 42 %). From 2091–2100 to 2291–2300, under the mitigation scenario RCP 2.6 the ensemble mean global burnt area and the respective CO_2 emissions slightly decrease, both by 5 % relative to their values in the period 2091–2100. In turn, under scenario RCP 4.5 (RCP 6.0, RCP 8.5) the ensemble mean burnt area in the period 2291–2100 is higher by 15 % (44 %, 83 %) than its mean value, and the ensemble mean CO_2 emissions are correspondingly higher by 9 % (19 %, 31 %). The simulated changes of natural fire characteristics in the 21st–23rd centuries are associated mostly with the corresponding changes in boreal regions of Eurasia and North America. However, under the RCP 8.5 scenario, the increase of the burnt area and CO_2 emissions in boreal regions during the 22nd and 23rd centuries is accompanied by the respective decreases in the tropics and subtropics.

1 Introduction

One of the most important recent achievements in global environmental modelling is an implementation of biogeochemistry modules in global climate models which converted the latter to Earth system models (e.g. Ciais et al., 2013). An important part of the terrestrial biogeochemistry modules is a scheme simulating natural fires. The first of such schemes was the GlobFIRM (Global FIRe Model) (Thonicke et al.,

2001). This scheme is based on statistical description of natural fires relating length of fire season, and the burnt area to environmental variables (soil moisture content and carbon stocks) via specified functional relationships. This model was implemented into the LPJ (Lund–Potsdam–Jena) terrestrial vegetation model (Sitch et al., 2003). The GlobFIRM was followed by the scheme developed at the Canadian Centre for Climate Modelling and Analysis (CCCMA) (Arora and Boer, 2005). Comparing to the Glob–FIRM model, the latter scheme accounts for (i) an impact of both natural and anthropogenic ignition sources on fire occurrence, and (ii) an influence of wind direction and speed on fire propagation. This scheme was implemented in the CCCMA global climate model and, in a slightly changed version, in the CLM-3.5 land-surface model (Common Land Model, version 3.5) (Kloster et al., 2010, 2012). Li et al. (2012) developed an intermediate complexity scheme to calculate characteristics of natural fires, which is an extension of the CCCMA scheme. To date, the most advanced scheme for simulation of natural fires in global climate models is the SPITFIRE (Spread and Intensity of FIRE) model (Thonicke et al., 2010) which is able to calculate even the detailed characteristics of natural fires. Currently, the SPITFIRE superseded the GlobFIRM in the LPJ model.

At present, the global-scale natural fire modelling is far from its mature stage. For instance, the SPITFIRE model, forced by the gridded atmospheric observations, generally underestimates the burnt area in the tropics and overestimates it in the middle latitudes (Thonicke et al., 2010). The simulation results with the CLM-3.5 model, which is also forced by the gridded atmospheric observations, show strong dependence on the chosen parametrisation of fire processes (Kloster et al., 2010). In particular, depending on the chosen parametrisation, the burnt area in the extratropics (where influence of the anthropogenic fires is small) may be either under- or overestimated. The same statement is valid for the emissions from fires simulated by the CLM-3.5.

Natural fires release a number of greenhouse gases and aerosols into the atmosphere (e.g. Crutzen et al., 1985; Andreae and Merlet, 2001; van der Werf et al., 2010; Konovalov et al., 2011; Elansky et al., 2011; Ciais et al., 2013; Turquety et al., 2014) and affect functioning of ecosystems (e.g. Hughes et al., 2000; Thonicke et al., 2010; Ciais et al., 2013). All of this might affect the atmosphere and terrestrial biosphere (Ward et al., 2012), feeding back to characteristics of natural fires. The strength of the latter feedback is not known a priori and could be estimated only by using coupled Earth system models incorporating schemes simulating natural fires and their impact on radiative transfer, cloud and precipitation formation, atmospheric chemistry, dynamics, terrestrial vegetation, etc.

At present, the values of some important parameters of natural fire schemes are known with insufficient precision, and frequently they are just tuned to achieve a reasonable performance of a particular model. In principle, the best way to

constrain the model parameters would be to solve a relevant inverse problem by using available observations. However, this is not easily achieved in practice because to invert a numerical model is not a readily solvable task. Moreover, measurements obtained at different geographical locations and/or at different time intervals, in principle, for a given scheme simulating natural fires, may lead to the values of the same parameter which contradict each other. This is a consequence of assumptions and simplifications of the latter scheme. In this case, one of two paths could be followed. The first one is to increase the complexity of a scheme. However, this way may be hindered by either insufficient knowledge on relevant processes or by details of the Earth system model for which a particular natural fires scheme is developed. This is valid, for instance, for the Earth system models of intermediate complexity. Thus, the second method should be followed, which is to adopt a compromise in the model's performance in different regions and/or at different time intervals.

The goal of the present paper is to suggest and test an approach to achieve such a compromise. Namely, we suggest to sample the values of the model's parameters, constrain these simulations by available observations, calculate ensemble statistics, and consider ensemble means and standard deviations as central values of characteristics of natural fires and their uncertainties, respectively (Fig. 1).

In our paper, the scheme for simulation characteristics of natural fires, which is a descendant of the GlobFIRM model, is implemented in an Earth system model. The latter allows us to put these simulations in the context of the climate changes occurring at present and expected in the next few centuries. We force our coupled model by anthropogenic and natural forcings scenarios for the period AD 850–2100 (hereafter all years are taken as being AD). These scenarios are prepared for the CMIP5 (Coupled Models Intercomparison Project, phase 5) simulations with Earth system models. We note that, while the "core" CMIP5 simulations end in 2100, the "tier 1" and "tier 2" ones are extended until the year 2300 (Taylor et al., 2012). In all these simulations, the anthropogenic forcing is stabilised not later than in the mid-22nd century, but climate inertia may lead to pronounced changes in climate state for decades and even centuries after such a stabilisation, and, consequently, to changes in characteristics of natural fires. So, it is profitable to extend our simulations for the whole period covered by the CMIP5 scenarios to study the possible impact of delayed climate changes on simulation of natural fires. The large computation burden, involved in our exercise, precludes us from using the detailed state-of-the-art climate model, and thus we use the global climate model of intermediate complexity. In turn, because the latter model is unable to provide the necessary information for the detailed scheme for simulating natural fires, we use a simplified (albeit realistic at global and continental scales) natural fire module based on the GlobFIRM model.
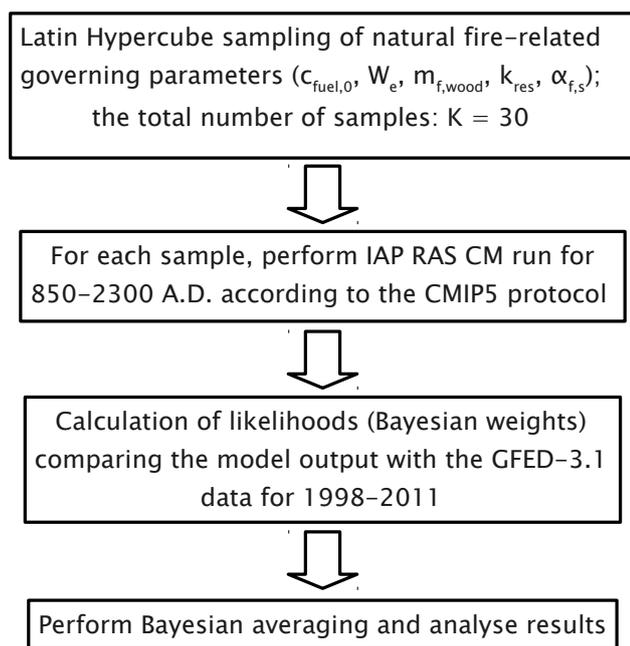
Latin Hypercube sampling of natural fire–related governing parameters ($c_{fuel,0}$, W_e, $m_{f,wood}$, k_{res}, $\alpha_{f,s}$); the total number of samples: K = 30

⬇

For each sample, perform IAP RAS CM run for 850–2300 A.D. according to the CMIP5 protocol

⬇

Calculation of likelihoods (Bayesian weights) comparing the model output with the GFED–3.1 data for 1998–2011

⬇

Perform Bayesian averaging and analyse results

Figure 1. The general flow chart.

2 Methods

2.1 IAP RAS global climate model

In this paper, the global climate model (CM) developed at the A. M. Obukhov Institute of Atmospheric Physics, Russian Academy of Sciences (IAP RAS) (Petoukhov et al., 1998; Mokhov et al., 2002, 2005; Mokhov and Eliseev, 2012) is used. It belongs to the class of the Earth system models of intermediate complexity (Claussen et al., 2002; Petoukhov et al., 2005; Eby et al., 2013; Zickfeld et al., 2013). An initial implementation of the natural fire module as a part of the IAP RAS CM's terrestrial carbon cycle module is described by Eliseev and Mokhov (2011a), further extensions are reported by Eliseev (2012) and by Eliseev and Sergeev (2014). The IAP RAS CM resolution is 4.5° in latitude and 6° in longitude. Therefore, we note a possible gap in spatial scales between the GFED-3.1 data (approx. 1 km) and our model.

The model's terrestrial vegetation module distinguishes seven plant functional types (PFTs): tropical trees, temperate broadleaf trees, cool needleleaf trees, grasses, shrubs, wetlands, and crops. To allow two or more PFTs coexist in a model grid cell, a mosaic approach is used (Eliseev and Sergeev, 2014). Fractional areas occupied by PFTs are prescribed and do not respond to natural fire activity in the model. However, they are allowed to evolve in time according to external deforestation/afforestation scenarios. Seasonal changes of all variables which serve as an input for the terrestrial vegetation module are considered explicitly, but the analysis in the present paper is restricted to annual means. Vegetation carbon is divided in two pools: the "leave"

pool representing leaves, thin branches and thin roots, and the "wood" pool representing thick branches, thick roots, and hardwood.

The model implements a statistical module to simulate characteristics of natural fires, which is a descendant of the GlobFIRM model (Thonicke et al., 2001). In this model, the fractional (relative to the area occupied by a given PFT in a given grid cell) burnt area is calculated as a function of soil moisture and available fuel stock. The whole "leave" carbon pool in this burnt part of the cell is consumed completely during fires. The respective amount of the consumed "wood" pool depends on PFT (see Eliseev and Sergeev, 2014, for more details). The GlobFIRM model was selected for implementation in the IAP RAS CM because the complexity of these two models are in approximate correspondence to each other.

For the present paper, the model's natural fires module is extended by a simple parametrisation of peat fires. If, during a time step and in a given grid cell, natural fires consume vegetation carbon mass per unit area δc_v, they also consume carbon in soil. The latter consumption per unit area in our model is applied only if the total soil carbon stock is larger than $c_s > c_{s,0} = 10\,\mathrm{kg\,C\,m^{-2}}$ and reads

$$\delta c_s = \alpha_{f,s}\delta c_v(1 - W), \tag{1}$$

where $\alpha_{f,s}$ is a coefficient, and W is moisture fractional saturation of the upper soil level. The value of the threshold $c_{s,0}$ is chosen as a typical value distinguishing the peat and non-peat soils. The precise value of this threshold should depend either on the resolution of input data or on the size of the model grid cell. The ISLSCP II (International Satellite Land Surface Climatology Project, Initiative II) data for soil carbon stock interpolated on the IAP RAS CM grid resolution was reported by Eliseev and Mokhov (2011a, their Fig. 7b). The threshold value $10\,\mathrm{kg\,C\,m^{-2}}$ was chosen by a visual inspection of those data. This value should be larger at a finer resolution. For instance, the high-resolution (nominally, 150 m) data for the West Siberian Lowlands (Sheng et al., 2004) support the threshold value as large as $30\,\mathrm{kg\,C\,m^{-2}}$. It is assumed in Eq. (1) that soil carbon is consumed during fires only if the soil fuel stock is sufficiently large. Based on the latter, we assume that fire development is limited by environmental factors rather than by the available soil fuel stock. For this reason, c_s does not enter the right-hand side of Eq. (1). Further, δc_v heuristically represents an overall severity of fires in peatland regions. This severity, in turn, represents an ability of fires to penetrate into the soil. Some observational support for such a representation is given by Mack et al. (2011). In the latter paper, the carbon release from peat during a fire is related to the consumed amount of vegetation carbon. When burnt, both δc_s and δc_v are assumed to be emitted into the atmosphere in the form of carbon dioxide. As a result, total CO$_2$ emissions per unit area in the atmosphere due to natural

fires read

$$e = \delta c_{\rm v} + \delta c_{\rm s}. \tag{2}$$

This scheme for accounting a CO_2 release from soil during fires is similar (but not identical) to that employed in the CLM-3.5 (Li et al., 2013). In particular, they use a similar dependence of the CO_2 emissions from peat on soil moisture content, but directly relate the burnt area of peat to the area burnt by crown fires.

2.2 Simulations

Our simulations follow the CMIP5 protocol (Taylor et al., 2012). In particular, we performed "historical" simulations forced by the forcing reconstructions for the period 850–2005. This simulation was initialised from the model state occurring after a 200 yr spin-up with the forcing values corresponding to year 850. This simulation was continued till year 2300 forced by the RCP (Representative Concentration Pathway) scenarios. All scenarios RCP 2.6, RCP 4.5, RCP 6.0, and RCP 8.5 (see Moss et al., 2010) were used in our paper. We employed forcings due to three well-mixed atmospheric greenhouse gases (GHGs; namely, CO_2, N_2O, and CH_4), tropospheric and stratospheric sulfate aerosols (only direct forcing), change in surface albedo due to land use, and total solar irradiance. For carbon dioxide, we prescribed fossil fuel + industrial CO_2 emissions and computed the respective land use emissions by the model's terrestrial carbon cycle scheme based on change of extent of crops and pastures. Carbon dioxide content in the atmosphere was calculated interactively by the IAP RAS CM as well. For other well-mixed GHGs (N_2O and CH_4) atmospheric concentrations were used to force the model. Orbital forcing, possible change in vegetation types under climate changes, and changes in ozone burdens in the stratosphere and troposphere were neglected. Ice sheet distribution and heights were prescribed in the model.

All simulations were performed in an ensemble manner by varying the values of parameters of the natural fires module implemented in the IAP RAS CM:

– Fraction $m_{\rm f,\ wood}$ of carbon stock in hardwood and thick branches and thick woods consumed during fires. This parameter controls vegetation fuel stock available for fires:

$$c_{\rm fuel} = c_{\rm leaf} + m_{\rm f,\ wood}c_{\rm wood}, \tag{3}$$

where $c_{\rm leaf}$ is carbon stock in leaves and thin branches and roots, and $c_{\rm wood}$ is its counterpart in hardwood and thick branches and roots.

– Parameter $c_{\rm fuel,0}$, which is a threshold of fuel availability for natural fires, and below which these fires do not develop. In turn, the fuel stock is calculated as a linear function of carbon stock in leaves, fine branches and fine roots.

– Moisture of extinction $W_{\rm e}$, which controls the probability of fires to occur.

– Combustion completeness CC, which relates to CO_2 emissions from living vegetation due to natural fires, $e_{\rm v}$, and burnt vegetation fuel stock:

$$e_{\rm v} = \delta c_{\rm v} = {\rm CC} \cdot c_{\rm fuel}. \tag{4}$$

– Coefficient $\alpha_{\rm f,\ s}$ in Eq. (1).

In total, we sample 7 parameters as shown in Table 1. These parameters are $m_{\rm f,\ wood}$, $c_{\rm fuel,0}$, and $W_{\rm e}$ (which are non-PFT-dependent), CC (for grasses it is permanently set equal to unity and not sampled; and all other PFTs are merged in three groups, hence, we have three values), and $\alpha_{\rm f,\ s}$ (single value because it is sampled only for bogs/mires/fens; for all other PFTs it is permanently set equal to zero). All of these parameters were sampled by the Latin hypercube sampling (McKay et al., 1979; Stein, 1987). Their ranges and standard values adopted in the IAP RAS CM are listed in Table 1. The total sample size was $K = 30$, which is approximately an order of magnitude larger than the number of the sampled parameters. No other parameters were sampled and constrained in this paper.

Thereafter, performed simulations are labelled according to anthropogenic scenarios for the 21st–23rd centuries.

2.3 Post-processing

A Bayesian averaging of individual ensemble members (Kass and Raftery, 1995; Leroy, 1998; Hoeting et al., 1999) is employed in the present work. In particular, for each model variable or parameter Y, ensemble mean $\mathcal{E}(Y|D)$ and ensemble standard deviation $\sigma(Y|D)$, both conditioned by data set D, are computed, respectively, as follows:

$$\mathcal{E}(Y|D) = \sum_{k=1}^{K} Y_k w_k \tag{5}$$

and

$$\sigma(Y|D) = \left\{ \sum_{k=1}^{K} \left[\sigma_k^2 + Y_k^2 \right] w_k - \mathcal{E}(Y|D)^2 \right\}. \tag{6}$$

Here Y_k is output for the ensemble member M_k ($k = 1, \ldots, K$), σ_k is standard deviation of natural variability generated by the model, and w_k is the weight attached to this ensemble member. Because our model, similar to other Earth system models of intermediate complexity, underestimates natural variability, we set $\sigma_k = 0$ in Eq. (7).

Bayesian weights w_k's are calculated by comparing the modelled emissions due to natural fires e with their observational counterparts. These weights are constructed based on two figures depicting global total emissions, $w_{\rm g,k}$, and spatial structure of fire emissions, $w_{\rm s,k}$:

$$w_k \propto w_{\rm g,k} w_{\rm s,k}. \tag{7}$$

Table 1. Standard values, sampling ranges, and posterior distributions of variables varied within the ensemble constructed in this paper. In the first column, ND stands for non-dimensional. The plant functional types (PFTs) are TT – tropical trees, EDT – extratropical deciduous trees, ENT – extratropical evergreen (needleleaf) trees, GRA – grasses, SHR – shrubs, WTL – bogs/mires/fens, CRO – crops. Long dashes in the last two columns indicate that respective parameter is not sampled for a given PFT.

Variable	PFTs	Standard value	Sampling range	Posterior distribution
$c_{\mathrm{fuel},0}$, $\mathrm{kg\,C\,m^{-2}}$	all	0.2	0.1–0.3	0.21 ± 0.07
W_{e}, ND	all	0.7	0.4–0.8	0.56 ± 0.03
$m_{\mathrm{f,wood}}$, ND	all	0.2	0.15–0.50	0.36 ± 0.10
CC, ND	TT, EDT	0.5	0.25–0.75	0.51 ± 0.10
	ENT, SHR, WTL	0.12	0.1–0.2	0.15 ± 0.04
	CRO	0.1	0–0.2	0.12 ± 0.05
	GRA	1	–	–
$\alpha_{\mathrm{f,s}}$, ND	WTL	2	0–4	2.1 ± 0.8
	all other	0	–	–

The first is calculated assuming normal distribution of modelling bias in E_{g} (here and below, E depicts the value of e_{f} summed over a given region and the subscript indicates this region, "global" in the present example):

$$w_{\mathrm{g},k} = \left(2\pi \sigma_{\mathrm{g,o}}^2\right)^{-1/2} \exp\left(-\frac{\left(E_{\mathrm{g}} - E_{\mathrm{g,o}}\right)^2}{2\sigma_{\mathrm{g,o}}^2}\right). \tag{8}$$

Here the subscript "o" stands for the observed values, $\sigma_{\mathrm{g,o}}$ is sampled standard deviation of global CO_2 emissions due to natural fires. In turn, $w_{k,\mathrm{s}}$ is computed as in Taylor (2001):

$$w_{\mathrm{s},k} = \frac{(1+r)^4}{\left(a_{\mathrm{rel}}^2 + a_{\mathrm{rel}}^{-2}\right)}. \tag{9}$$

In Eq. (9), r is the coefficient of spatial correlation between area-weighted modelled and observed fields of CO_2 emissions due to fires, and a_{rel} is the so-called relative spatial variation which reads

$$a_{\mathrm{rel}} = a/a_{\mathrm{o}}, \tag{10}$$

where a^2 is the spatial (area weighted) average of $\left(e - E_{\mathrm{g}}/A_{\mathrm{g}}\right)^2$, and A_{g} is the area of Earth's surface. In turn, a_{o} is defined similar to a but for the observed field. To apply Eqs. (5) and (6), weights are standardised assuring that $\sum_{k=1}^{K} w_k = 1$.

The GFED-3.1 (van der Werf et al., 2010) for the period 1997–2010 data set is used to compute the Bayesian weights. Only natural fires (classified either "grassland and open savanna fires", "woodland fires", "forest fires", or "peat fires" in this database) are used to calculate the Bayesian weights. In addition, because CO_2 emissions due to peat fires were extremely large in year 1997 ($0.7\,\mathrm{Pg\,C\,yr^{-1}}$ while in other years they never exceeded $0.2\,\mathrm{Pg\,C\,yr^{-1}}$), we redid all our calculations excluding year 1997 from the computation of Bayesian weights. No marked differences between these two approaches were found, and further all

results are presented for the Bayesian weights calculated for the period 1998–2010. According to GFED-3.1 data, $E_{\mathrm{g,o}} = 1.4\,\mathrm{Pg\,C\,yr^{-1}}$, and $\sigma_{\mathrm{g,o}} = 0.2\,\mathrm{Pg\,C\,yr^{-1}}$. These numbers were used in Eq. (8) to obtain $w_{\mathrm{g},k}$. Once calculated based on the data for the period 1998–2011, the Bayesian weights are used to weight the members of the constructed ensemble for the whole simulation length.

To reduce an uncertainty related to the specific details of Bayesian weighting, we also made a projection in which all the members with weights $w_k \leq 1/K$ are dropped and only the sufficiently successful members are retained. Both qualitative and quantitative results are very similar between these two projections (compare Figs. 2–6 and Supplement Figs. S2–S6). Hence, we may conclude that the basic results of our paper are not sensitive to the Bayesian weighting specifics. However, the intra-ensemble standard deviation becomes smaller if the ensemble members with small weights are excluded from averaging. Further, only the original Bayesian averaging is discussed.

Thereafter, change of variable Y between different time periods, ΔY, is considered to be robust within the ensemble under study if magnitude of ensemble mean for this change is at least twice as large as the respective intra-ensemble standard deviation (Eliseev, 2011; Arzhanov et al., 2012):

$$|\mathcal{E}(\Delta Y | D)| \geq 2 \times \sigma(\Delta Y | D). \tag{11}$$

Below, we report only ensemble mean changes which are robust within the constructed ensemble.

Thereafter, we test our simulations against the GFED-3.1 data. We note, however, that these data, strictly speaking, contain information on all fires (both natural and anthropogenic), while we simulate only natural fires. Nevertheless, CO_2 emissions may be compared directly, because the GFED data contain fractions of emissions attributed to different sources. Unfortunately, no such information is available for the burnt area. To remove possible influence of anthropogenic fires on the burnt area, we masked out the grid

cells where the carbon release from anthropogenic fires, E_a, is larger than 5×10^{-4} g C m^{-2} yr^{-1}. The latter value was estimated by a visual inspection of the maps for E_a. The spatial distribution of the masked-out grid cells reasonably agrees with the combined distribution of the "deforestation" and "agriculture" fire types as published by van der Werf et al. (2010, their Fig. 13). Regional averages of the burnt area are calculated for the GFED data only for the regions where no grid cell was masked out. In addition, the simulated burnt area in the boreal zone is compared with the estimates by Conard et al. (2002) for year 1998. We note that the GFED data and the data (Conard et al., 2002) are not independent. In particular, both data sets for this year use the same fire identification algorithm based on the AVHRR (Advanced Very High Resolution Radiometer) data (Tucker et al., 2005) but differ between each other in the emission estimation algorithms.

Further, we "calibrated" parameters based on our ensemble simulations. This is done by the method suggested by Eliseev et al. (2013), where such a calibration was done by employing the Bayesian averaging (Eqs. 5, 6) but using parameter values in place of Y. In so doing, the Bayesian ensemble mean is considered as a central value, and the Bayesian intra-ensemble standard deviation is used as a substitute of the width of a range in which the simulation results are close to those obtained with a central parameter set.

3 Results

3.1 Calibrated values of parameters

The Bayesian weights for individual ensemble members are shown in Supplement Fig. S1. It is evident in this figure, that our ensemble is dominated by a few members. In particular, only four Bayesian weights are larger than $1/K = 1/30$, which is the value for the equally weighted averaging. The total weights w_k are closely related to $w_{g,k}$. In particular, the pairwise intra-ensemble Pearson correlation coefficients between w_k and $w_{g,k}$ equals to 0.99. In turn, the corresponding correlation coefficient between w_k and $w_{s,k}$ is only 0.15, which is statistically insignificant assuming that our ensemble weights are mutually independent (this assumption is well provided because of the Latin hypercube sampling) and sampled from the normal probability distribution (this assumption cannot be tested here because of insufficient sample size). An even smaller (equal to 0.12) correlation coefficient is found between $w_{g,k}$ and $w_{s,k}$. The latter allows us to consider $w_{g,k}$ and $w_{s,k}$ as variables which are mutually statistically independent, and, therefore, to use Eq. (7) to calculate the Bayesian weights.

The obtained values are shown in Table 1. All simulations with sufficiently large weights are characterised by moisture of extinction, W_e, which is close to 0.56. For instance, the ensemble members with $w_k \geq 0.01$ (which is approximately one-third of $1/K$) have $0.53 \geq W_e \geq 0.68$. However, the left tail of the posterior distribution for W_e is substantially shorter than the right one. The latter is due to relatively small sensitivity of our simulations to moisture of extinction when $W_e \geq 0.6$.

The values of other parameters affect the results of our simulations markedly less than values of W_e. In particular, for all other parameters p, the range with a centre in $\mathcal{E}(p|D)$ and of width $4 \times \sigma(p|D)$ (for normal distributions, this corresponds to the 95 % confidence interval) is close to that for the initial sampling range of this parameter (Table 1). The latter reflects a mutual redundancy between parameters. For instance, smaller CC may be compensated by increased $m_{f, wood}$. Another example of this redundancy is the compensation of smaller CO_2 emissions to the atmosphere (because of synergistic effect of CC and $m_{f, wood}$) by enhanced carbon dioxide emissions from the peat fires.

We note that the ensemble mean contribution of peat fires to the total CO_2 release in the atmosphere due to natural fires is small for all simulations reported in this paper.

3.2 Present-day burnt area and CO_2 emissions

In our ensemble, the global present-day (1998–2011) area burnt by natural fires is equal to $BA_g = (2.1 \pm 0.4) \times 10^6$ km^2 yr^{-1}, and the respective CO_2 emissions are $E_g = 1.4 \pm 0.2$ Pg C yr^{-1} (Table 2 and Fig. 2; here and below, the Bayesian ensemble mean and standard deviations are shown). The latter value agrees with the corresponding GFED-3.1 estimate of 1.4 ± 0.2 Pg C yr^{-1} (for the GFED data we show the interannual standard deviation). In different ensemble members, present-day BA_g (E_g) changes from 0.8×10^6 km^2 yr^{-1} to 5.8×10^6 km^2 yr^{-1} (from 0.3 Pg C yr^{-1} to 3.3 Pg C yr^{-1}). For ensemble members with $w_k \geq 1/K$ this range becomes markedly narrower: from 1.7×10^6 km^2 yr^{-1} to 2.4×10^6 km^2 yr^{-1} (from 1.2 Pg C yr^{-1} to 1.8 Pg C yr^{-1}) (Supplement Figs. S7 and S8).

The present-day burnt area BA per model grid cell ($4.5° \times 6.0°$, lat $\times$ long) is typically between 5×10^3 km^2 yr^{-1} and 10×10^3 km^2 yr^{-1} (Fig. 3a). Regions with a substantial fire activity are simulated in most parts of Africa and South America, in the southern part of Asia, and in the boreal zone of eastern Europe and Western Siberia. In these regions, there are hot spots with BA which is up to 50×10^3 km^2 yr^{-1}. All regions with BA $\geq 5 \times 10^3$ km^2 yr^{-1} are characterised by a relatively narrow intra-ensemble uncertainty of present-day fire area, since here $\sigma(s|D)/\mathcal{E}(s|D) \leq 0.3$ (Fig. 3c).

Comparing to the GFED data (Fig. 3e), the model correctly places large burnt areas in the subtropics of all continents. However, in these regions it generally underestimates BA. For instance, the latter in the region stretching from the Black Sea to the Aral Sea is markedly smaller in our model than in the GFED data. In addition, the burnt area in the region between Lake Baikal and the Pacific is underestimated as well. In turn, the burnt area in the Middle East is
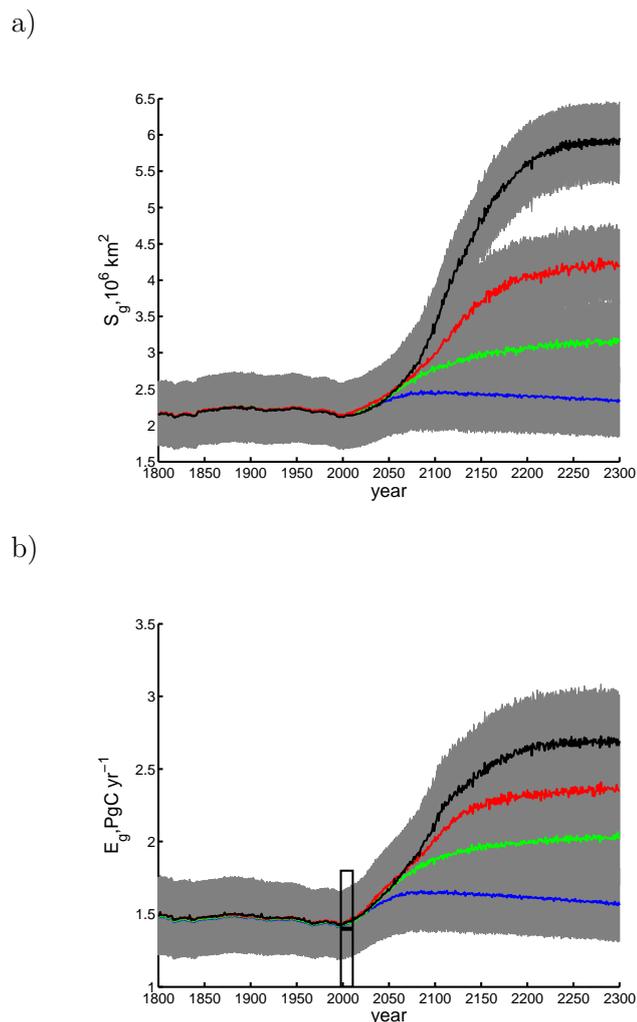
a)

b)

Figure 2. Ensemble mean of global natural-fire-burnt area **(a)** and respective CO_2 emissions to the atmosphere **(b)** in the simulations RCP 2.6, RCP 4.5, RCP 6.0, and RCP 8.5 (blue, green red, and black curves correspondingly) together with intra-ensemble standard deviations (gray shading). The rectangle in **(b)** represents the GFED-3.1 observations (mean and interannual standard deviation).

too large due to the overestimated fuel stock here. In addition, BA in the northern European Russia is larger than the GFED estimate because of the model's dry bias in this region (Arzhanov et al., 2008).

Spatial distribution of carbon dioxide emissions due to natural fires per unit area of a grid cell, e, is a product of the burnt area, fuel stock, and its flammability. Maxima of these emissions are simulated in the tropics and subtropics, where both BA and c_{fuel} are large. Here they are typically $e \geq 10\,\mathrm{g\,C\,m^{-2}\,yr^{-1}}$ and are frequently above $20\,\mathrm{g\,C\,m^{-2}\,yr^{-1}}$ (Fig. 3b). However, despite the large burnt area in the Near East, emissions are relatively small here, reaching several $\mathrm{g\,C\,m^{-2}\,yr^{-1}}$ because of the relatively small fuel stock in

these regions. Sizeable emissions ($10\,\mathrm{g\,C\,m^{-2}\,yr^{-1}} \leq e \leq 20\,\mathrm{g\,C\,m^{-2}\,yr^{-1}}$) are simulated for boreal regions in northern Europe, Western Siberia, north-eastern North America, and in Australia. In Europe, burnt area is small, but carbon dioxide emissions are noticeable. In most emission-prone regions $\sigma(e|D)/\mathcal{E}(e|D) \leq 0.3$ (Fig. 3d).

Comparing to the GFED-3.1 data (Fig. 3f), the extent of regions serving as emission sources in the model is too large in the tropics and subtropics. In turn, tropical sources are too low in comparison with the GFED data, sometimes by a factor of five. In the middle latitudes, the model simulates most emission sources in the north-eastern part of Europe, while in the GFED data these emissions mostly come from the north-eastern part of Asia. This may be either a model bias or a reflection of the interannual variability in natural fire activity which our model is unable to reproduce. One reason for such a bias may the neglect of fire suppression practices in our model. In particular, high population density and well-developed infrastructure in Europe can efficiently suppress natural fires in this region (Kloster et al., 2010). An incorporation of dependence of ignition source on population density might be a route to improve our model. In turn, interannual variability of fire activity could result in emissions which are larger than usual in eastern Asia in the period 1998–2011 relative to the previous years. We acknowledge that this point deserves future study.

Spatial distribution of the present-day burnt area and CO_2 emissions per grid cell in the tropics and subtropics changes little between different ensemble members with sufficiently large Bayesian weights (Supplement Figs. S7 and S8, left). We note, however, that there are ensemble members with a stronger emission source in the tropics (see the lowermost panels of these Figures as an example), while even in those members the tropical CO_2 source is still smaller than in the GFED data. Marked changes of the present-day BA are found between such members in the boreal zone. For instance, the clearly visible differences of this variable in boreal Eurasia are exhibited even for two ensemble members with the largest Bayesian weights: the ensemble member with $k = 4$ ($w_4 = 0.28$) and the member with $k = 15$ ($w_{15} = 0.32$). In particular, there are ensemble members with a weaker e in north-eastern Europe and stronger emissions in north-eastern Asia. The latter supports our observation that the discrepancy between the simulated and observed e is partly caused by interannual variability.

We calculated the sums of the burnt area and associated emissions over the regions chosen by the GFED team (see Supplement Fig. S9 and http://globalfiredata.org/pics/Fig7_BasisregionsMap.jpg). In most regions, for which it is possible to calculate regional averages based on the GFED data, our model basically overestimates the burnt area. The exceptions are BOAS (the Russian part of Asia and the northern part of European Russia), where agreement is reasonable, and AUST (Australia), where the burnt area is underestimated. If one compares BA_{BOAS} and

Table 2. Characteristics of natural fires in the simulations with the IAP RAS CM. For each variable, the burnt area BA and CO_2 emissions to the atmosphere E, the Bayesian ensemble mean and standard deviation are shown. The values for BA are in 10^6 square kilometres per year, and for E they are in petagrams of carbon per year. The regions correspond to the classification used by the GFED team as shown in Supplement Fig. S9. For the years 1998–2011, GFED-3.1 estimates (mean and interannual standard deviations) are shown in brackets; long dash stands for the absence of the latter estimate.

Variable	1998–2011	2090–2100			
		RCP 2.6	RCP 4.5	RCP 6.0	RCP 8.5
global					
BA	2.1 ± 0.4 (–)	2.4 ± 0.5	2.7 ± 0.5	2.9 ± 0.5	3.2 ± 0.5
E	1.4 ± 0.2 (1.4 ± 0.2)	1.6 ± 0.3	1.9 ± 0.3	2.0 ± 0.3	2.1 ± 0.3
BOAS					
BA	0.17 ± 0.05 (0.07 ± 0.04)	0.35 ± 0.08	0.55 ± 0.07	0.66 ± 0.09	1.00 ± 0.07
E	0.07 ± 0.02 (0.11 ± 0.09)	0.14 ± 0.03	0.22 ± 0.04	0.28 ± 0.06	0.39 ± 0.07
CEAS + SEAS + EQAS					
BA	0.35 ± 0.06 (–)	0.38 ± 0.07	0.39 ± 0.08	0.39 ± 0.08	0.40 ± 0.08
E	0.25 ± 0.04 (0.10 ± 0.05)	0.28 ± 0.05	0.29 ± 0.05	0.30 ± 0.05	0.31 ± 0.05
AUST					
BA	0.17 ± 0.03 (0.54 ± 0.24)	0.17 ± 0.03	0.17 ± 0.03	0.17 ± 0.03	0.16 ± 0.03
E	0.08 ± 0.01 (0.12 ± 0.04)	0.08 ± 0.01	0.08 ± 0.01	0.08 ± 0.01	0.08 ± 0.01
BONA					
BA	0.07 ± 0.02 (0.02 ± 0.01)	0.11 ± 0.03	0.13 ± 0.03	0.18 ± 0.03	0.21 ± 0.05
E	0.05 ± 0.01 (0.05 ± 0.03)	0.08 ± 0.02	0.11 ± 0.02	0.12 ± 0.02	0.14 ± 0.03
TENA + CENA + NHSA					
BA	0.20 ± 0.05 (0.05 ± 0.01)	0.21 ± 0.05	0.21 ± 0.05	0.21 ± 0.05	0.21 ± 0.05
E	0.18 ± 0.06 (0.03 ± 0.02)	0.20 ± 0.06	0.21 ± 0.07	0.22 ± 0.07	0.22 ± 0.07
SHSA					
BA	0.24 ± 0.04 (–)	0.24 ± 0.04	0.24 ± 0.04	0.24 ± 0.04	0.24 ± 0.04
E	0.26 ± 0.04 (0.12 ± 0.06)	0.28 ± 0.05	0.29 ± 0.05	0.30 ± 0.05	0.30 ± 0.05
EURO					
BA	0.04 ± 0.01 (0.01 ± 0.01)	0.05 ± 0.01	0.07 ± 0.01	0.09 ± 0.02	0.11 ± 0.02
E	0.02 ± 0.01 (0.01 ± 0.01)	0.04 ± 0.01	0.05 ± 0.01	0.05 ± 0.01	0.06 ± 0.01
MIDE					
BA	0.44 ± 0.12 (0.01 ± 0.01)	0.46 ± 0.14	0.51 ± 0.15	0.51 ± 0.13	0.48 ± 0.14
E	0.14 ± 0.02 (0.001 ± 0.001)	0.15 ± 0.02	0.17 ± 0.02	0.17 ± 0.03	0.16 ± 0.03
NHAF					
BA	0.32 ± 0.05 (–)	0.31 ± 0.05	0.32 ± 0.05	0.34 ± 0.06	0.28 ± 0.05
E	0.23 ± 0.03 (0.38 ± 0.06)	0.24 ± 0.03	0.26 ± 0.03	0.29 ± 0.04	0.22 ± 0.03
SHAF					
BA	0.14 ± 0.03 (–)	0.14 ± 0.03	0.14 ± 0.03	0.14 ± 0.03	0.14 ± 0.03
E	0.15 ± 0.03 (0.49 ± 0.04)	0.16 ± 0.03	0.17 ± 0.04	0.17 ± 0.04	0.17 ± 0.04

BA_{BONA} ((0.17 ± 0.05) $\times 10^6$ km^2 yr^{-1} and (0.07 ± 0.02) $\times 10^6$ km^2 yr^{-1} correspondingly; Table 2) with the numbers reported by Conard et al. (2002) (0.12×10^6 km^2 yr^{-1} and 0.03×10^6 km^2 yr^{-1}, respectively) the conclusion remains basically unchanged. However, the correspondence between the GFED regions and the regions chosen by Conard et al. (2002) is unclear. In our model, the largest contribution to BA_g is found for region MIDE (northern Africa and the Middle East; Table 2) with the next equally important contri-

butions from region NHAF (the northern tropics of Africa; Fig. 4a) and from the combined region CEAS+EQAS+SEAS (which is the greater part of Asia excluding boreal regions and the Middle East). The contribution of boreal regions, BOAS and BONA (the latter combines Canada and Alaska), to the present-day BA_g is small (Fig. 4c, e).

About one-half of E_g comes from the regions SHSA (Africa southward from the Equator), CEAS+EQAS+SEAS, and NHAF. Comparing with
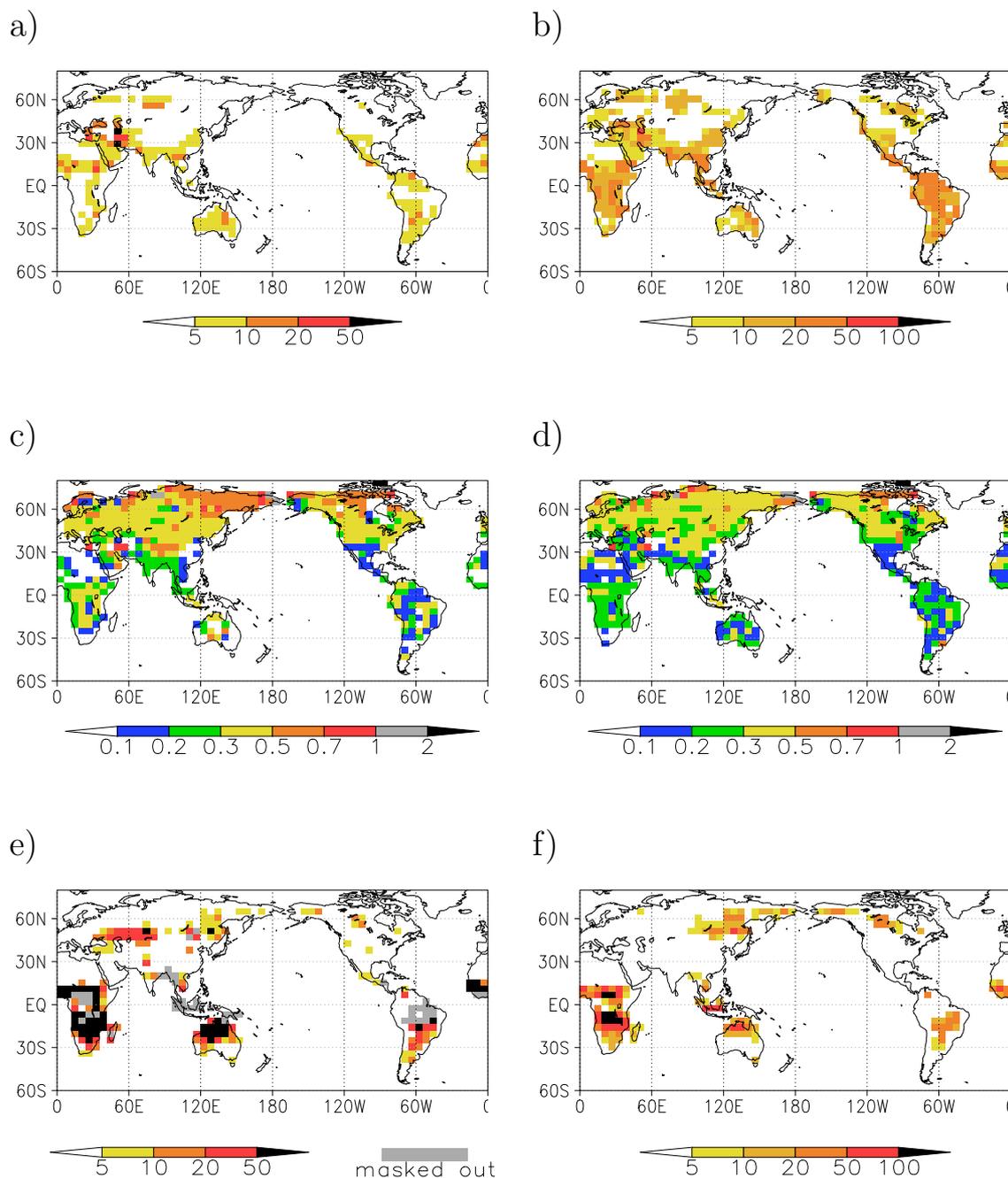
Figure 3. Area annually burnt by natural fires (**a** and **c**), and corresponding CO_2 emissions in the atmosphere (**b** and **d**) simulated by the IAP RAS CM for years 1998–2011. Shown are the Bayesian ensemble means (burnt area in 10^3 km^2 yr^{-1} per grid cell (**a**) and emissions in g C m^{-2} yr^{-1}) (**b**) and the ratios of the Bayesian standard deviations to the Bayesian ensemble means (**c**) and (**d**). In addition, the GFED-3.1 estimates are shown in (**e**) and (**f**). In panel (**e**) grid cells with CO_2 emissions $\geq 5 \times 10^{-4}$ g C m^{-2} yr^{-1} due to anthropogenic fires are masked out.

the GFED data, emissions from these regions are reproduced reasonably (e.g. Fig. 4b). Other regions with an important contribution to E_g are TENA + CENA + NHSA (which combines the southern part of North America and the northern part of South America), MIDE, and SHAF (the southern tropics of Africa). However here the modelled CO_2

emissions due to natural fires in the first two regions are much larger than the GFED estimates, and in the third region they are much smaller than this estimate. For the boreal regions, BOAS and BONA, our model realistically simulates the present-day regionally averaged annual CO_2 emissions (Table 2; Fig. 4d, f). They are also in general agreement with
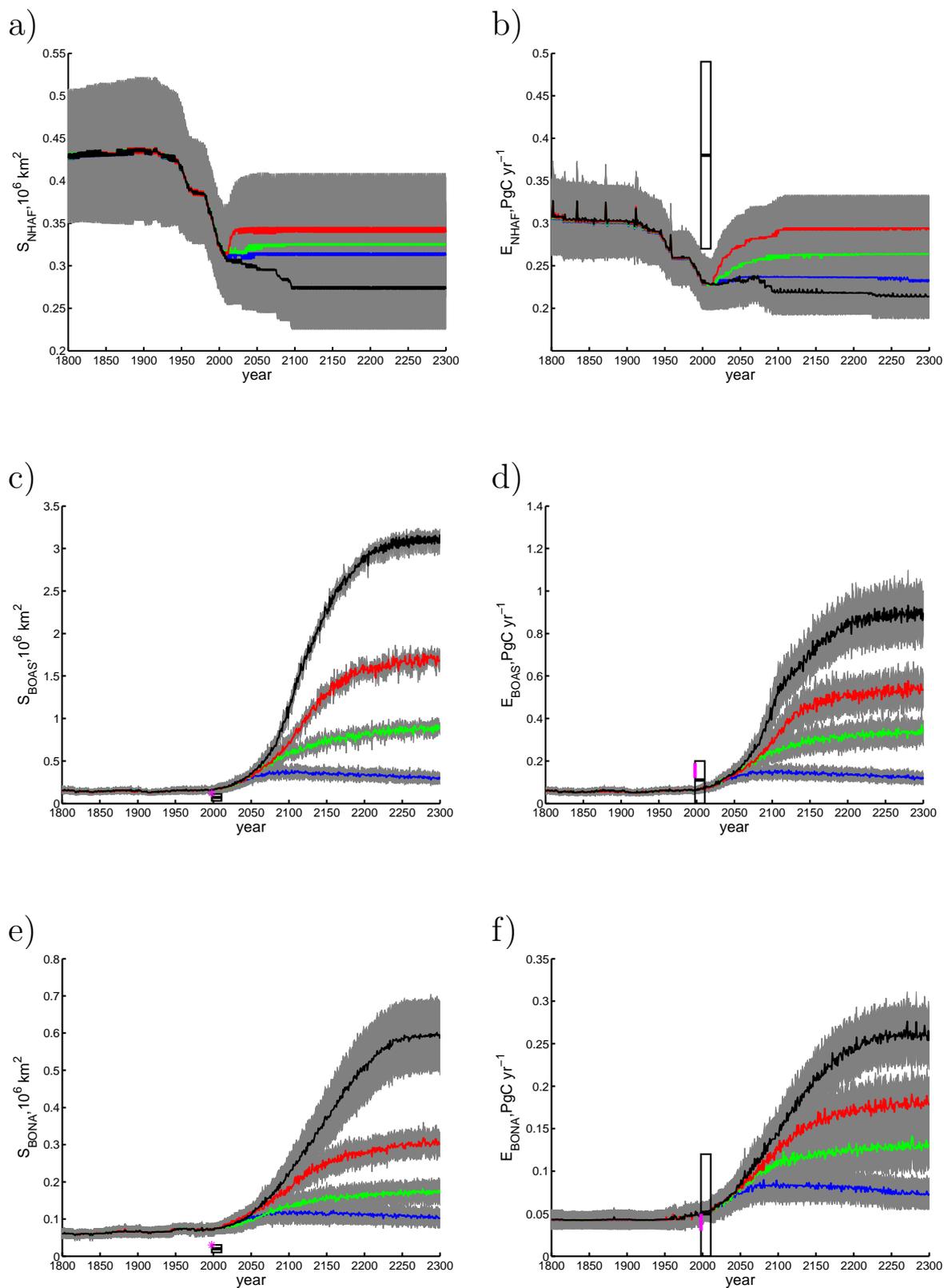
Figure 4. Similar to Fig. 2, but for the burnt area (**a**, **c**, and **e**) and respective CO_2 emissions (**b**, **d**, and **f**) summed over the GFED regions NHAF (**a** and **b**), BOAS (**c** and **d**), and BONA (**e** and **f**). The GFED regions are shown in Supplement Fig. S9. Magenta symbols are used for estimates by Conard et al. (2002): the star is for the burnt area and the line is for the emissions (line width represents uncertainty range).

the estimates by Conard et al. (2002) (from $0.12\,\mathrm{Pg\,C\,yr^{-1}}$ to $0.19\,\mathrm{Pg\,C\,yr^{-1}}$ and from $0.03\,\mathrm{Pg\,C\,yr^{-1}}$ to $0.05\,\mathrm{Pg\,C\,yr^{-1}}$ respectively; the discrepancy for region BOAS may be caused by the above-mentioned imprecise correspondence of this region to the region chosen by Conard et al. (2002)).

3.3 Changes in the 21st century

By the end of the 21st century (2091–2100), the global burnt area increases to $(2.4 \pm 0.5) \times 10^6\,\mathrm{km^2\,yr^{-1}}$ under scenario RCP 2.6, to $(2.7 \pm 0.5) \times 10^6\,\mathrm{km^2\,yr^{-1}}$ under scenario RCP 4.5, to $(2.9 \pm 0.5) \times 10^6\,\mathrm{km^2\,yr^{-1}}$ under scenario RCP 6.0, and to $(3.2 \pm 0.5) \times 10^6\,\mathrm{km^2\,yr^{-1}}$ under scenario RCP 8.5 (Fig. 2a). These changes correspond to increases of the ensemble mean BA_g relative to its value in the period 1998–2010 by 13 %, 28 %, 36 %, by 51 % respectively. A proportional change is simulated for E_g which attains in year 2100 $1.6 \pm 0.3\,\mathrm{Pg\,C\,yr^{-1}}$ under scenario RCP 2.6, $1.9 \pm 0.3\,\mathrm{Pg\,C\,yr^{-1}}$ under scenario RCP 4.5, $2.0 \pm 0.3\,\mathrm{Pg\,C\,yr^{-1}}$ under scenario RCP 6.0, and $2.1 \pm 0.3\,\mathrm{Pg\,C\,yr^{-1}}$ under scenario RCP 8.5 (Fig. 2b). In relative units, the ensemble mean E_g is higher in the period 2091–2100 with respect to its value for years 1998–2011 by 14 % under scenario RCP 2.6, by 29 % under scenario RCP 4.5, by 37 % under scenario RCP 6.0, and by 42 % under scenario RCP 8.5.

For all scenarios, a general increase of the burnt area in the 21st century is caused by an increase of BA on boreal regions of Eurasia and North America (Fig. 5, left panels). In particular, in the BOAS region, the ensemble mean burnt area is doubled during the 21st century under scenario RCP 2.6, tripled under scenario RCP 4.5, quadrupled under scenario RCP 6.0, and increased fivefold under scenario RCP 8.5 (Fig. 4b). A relative increase in the regions BOAS and EURO (the latter is the part of Europe excluding the former Soviet Union) is more modest. However, the year 2100 values of both BA_BOAS and BA_EURO are larger than the respective present-day values by more than one-third under scenario RCP 2.6, and they are more than tripled under scenario RCP 8.5. In addition, under scenario RCP 8.5 there is a decrease of the burnt area in the northern tropics of Africa by about one-third of its present-day value (Figs. 4a, 5e).

The most important contribution to the simulated increase of the burnt area in the boreal regions is given by an increase of the fire season length. The latter in our model depends on upper soil moisture content W (drier soil increases fire probability) and on fuel stock c_fuel (an increase of fuel stock makes it easier to start the fire). In particular, in boreal North America both soil drying and fuel stock increase in the 21st century simulated by the IAP RAS CM under all the RCP scenarios (Fig. 7a–d). In the BOAS region, in contrast, soil as a whole becomes wetter during this century (while some grid cells with the decreasing W are visible in these regions in Fig. 7) and here the increase of the burnt area is basically related to the increase of c_fuel. The latter increase is responsible for the increase of BA_NHAF as well. We note that the

simulated increase of the fire season length in boreal Eurasia during the 21st century agrees with the results reported by Mokhov and Chernokulsky (2010) which were obtained by an application of a fire danger index to the output of the regional climate model.

The direction of change of CO_2 emissions per unit area of a grid cell is rather similar to its burnt area counterpart (Fig. 6, left panels). In particular, the model simulates a very pronounced enhancement of CO_2 emissions due to fires in boreal regions of Eurasia and North America. We note, however, that, in contrast to BA, the region of the robust increase of e in the 21st century is simulated over the north-eastern part of Eurasia as well. This is caused by both the above-mentioned increase of the burnt area in these regions and by the respective increase of the carbon stock in living vegetation (the latter is reported by Mokhov and Eliseev, 2012) resulting in increased fuel stock. In addition, a decrease of CO_2 emissions in the northern tropics of Africa in the 21st century under scenario RCP 8.5 is less visible than its burnt area counterpart. This is a product of a diminished burnt area and an increased carbon stock in living vegetation.

Both the burnt area and the release of the carbon dioxide in the atmosphere due to natural fires are quite robust within the studied ensemble. In particular, the changes of both the burnt area and the associated CO_2 release to the atmosphere are similar between the ensemble members with sufficiently high Bayesian weights (Supplement Figs. S7 and S8, right panels).

To date, no results on the response of natural fire characteristics to the 21st–23rd centuries' climate changes have been reported for other Earth system models. However, we may compare our results with the results obtained in offline calculations performed with the CLM-3.5 as reported by Kloster et al. (2012). The CLM-3.5 was forced by the climate anomalies simulated by two general circulation models (GCMs), ECHAM5/MPI–OM and CCSM, and by the land use forcing prescribed according to the RCP scenarios (for more details see Kloster et al., 2012). The GCM simulations were performed under the SRES (Special Report on Emission Scenarios) A1B scenario of anthropogenic forcing (Nakićenović et al., 2000) which is comparable to the RCP 6.0 scenario. As reported by Kloster et al. (2012, their Table 2), in the CLM-3.5 simulation E_g increased during the 21st century by 22–66 % depending on the GCM output. Our increase obtained under scenario RCP 6.0, 37 %, is in the central part of this range. In addition, Kloster et al. (2012) have also obtained a threefold to fourfold increase of E_BONA and a sixfold to eightfold increase of E_BOAS during the same century, which are even larger (in relative units) than those in our simulations. For the EURO region, our approximately twofold increase of CO_2 emissions from natural fires during the 21st century is comparable to the values reported by Kloster et al. (2012) (a 2–2.5-fold increase). For other regions, our results are comparable with the results published in Kloster et al. (2012) as well.
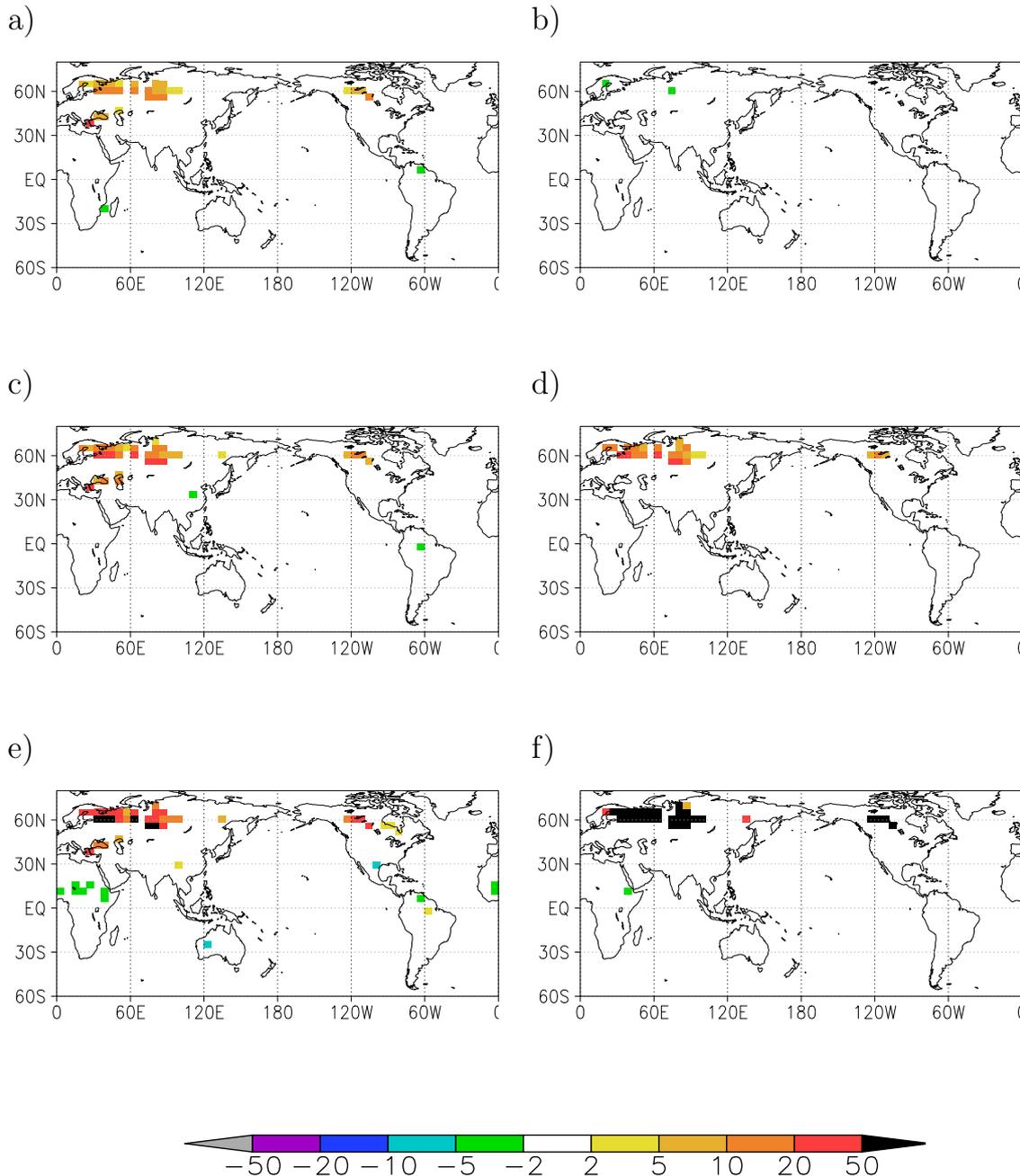
Figure 5. Change of the area annually burnt by natural fires (10^3 km^2 yr^{-1} per grid cell) from 1998–2011 to 2090–2100 (**a**, **c**, and **e**) and from 2090–2100 to 2290–2300 (**b**, **d**, and **f**) in simulations RCP 2.6 (**a** and **b**), RCP 4.5 (**c** and **d**), and RCP 8.5 (**e** and **f**).

3.4 Changes in the 22nd and 23rd centuries

Under the mitigation scenario RCP 2.6, BA$_g$ and E_g start to decrease around year 2100, and reach in the late 23rd century (2291–2100) $(2.3 \pm 0.5) \times 10^6$ km^2 yr^{-1} and 1.6 ± 0.2 Pg C yr^{-1} correspondingly (Fig. 2). Both values are decreased by about 5 % relative to their values in the period 2091–2100. Under other scenarios, both the burnt area and global CO_2 emissions form natural fires con-

tinue to increase. In our model, BA$_g$ achieves in the period 2291–2300 $(3.2 \pm 0.6) \times 10^6$ km^2 yr^{-1} for scenario RCP 4.5, $(4.2 \pm 0.5) \times 10^6$ km^2 yr^{-1} for scenario RCP 6.0, and $(5.9 \pm 0.5) \times 10^6$ km^2 yr^{-1} for scenario RCP 8.5. This corresponds to the ensemble mean increase relative to the value in the period 2091–2100 by 15 %, 49 % and 83 %, respectively. In turn, E_g is increased by 9 % under scenario RCP 4.5, by 19 %, under scenario RCP 6.0, and by 31 % under scenario RCP 8.5. The simulated global CO_2
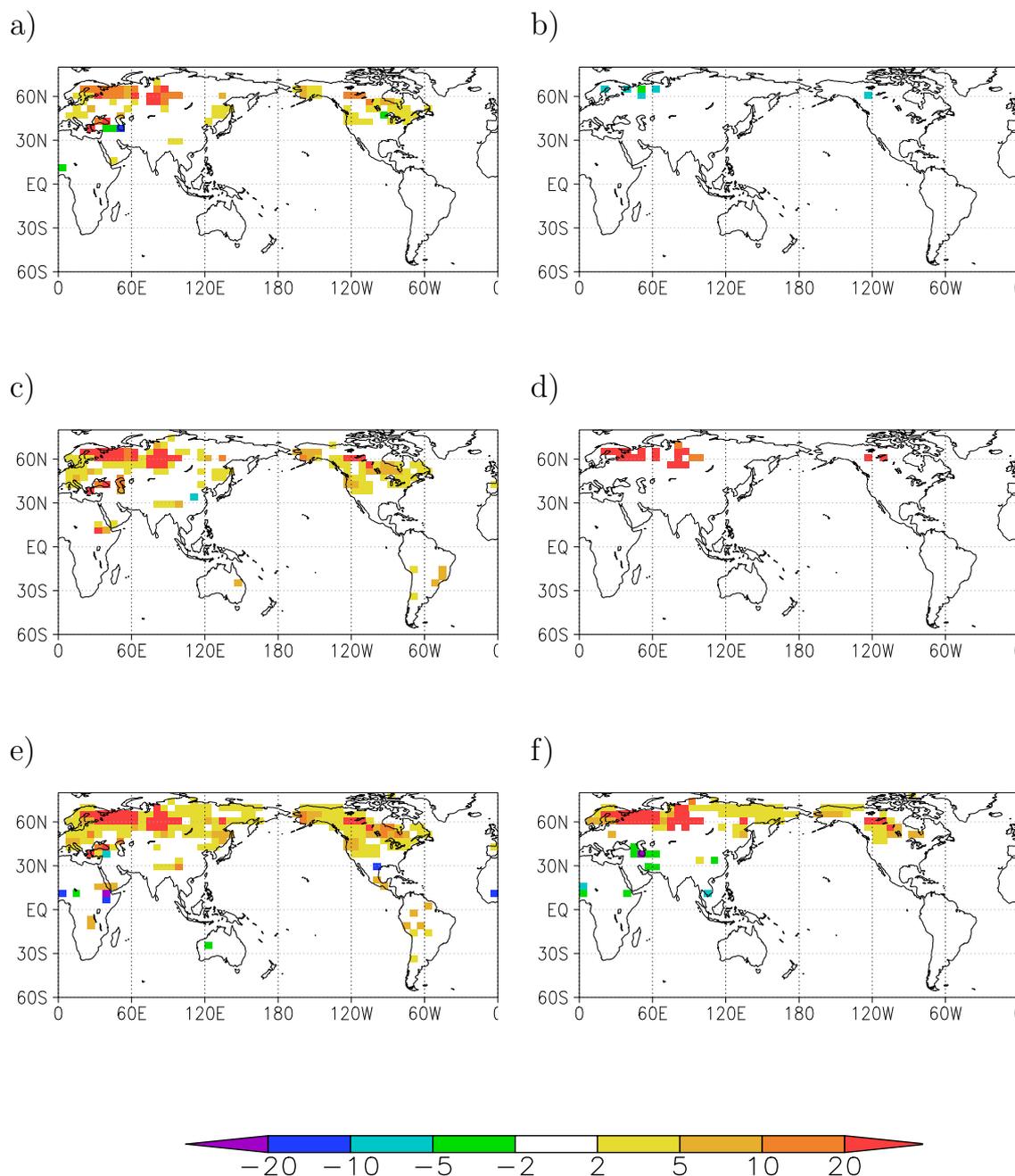
Figure 6. Similar to Fig. 5, but for the corresponding CO_2 emissions to the atmosphere ($\mathrm{g\,C\,m^{-2}\,yr^{-1}}$).

emissions from natural fires in the late 23rd century are $2.0 \pm 0.3\,\mathrm{Pg\,C\,yr^{-1}}$ for scenario RCP 4.5, $2.4 \pm 0.3\,\mathrm{Pg\,C\,yr^{-1}}$ for scenario RCP 6.0, and $2.7 \pm 0.3\,\mathrm{Pg\,C\,yr^{-1}}$ for scenario RCP 8.5.

In the 22nd and 23rd centuries, the burnt area and carbon emissions due to natural fires increase further in boreal regions of Eurasia and North America for scenarios RCP 4.5, RCP 6.0, and RCP 8.5 (Figs. 5, 6, right panels). This increase is more pronounced for scenarios with a higher anthropogenic carbon dioxide loading in the atmo-

sphere. For the mitigation scenario RCP 2.6, however, in these regions the model simulates a slight decrease of the burnt area and respective carbon dioxide release in the atmosphere (Figs. 5b, 6b). The latter is reflected in the above-mentioned small decrease of BA_g and E_g under this scenario in this period. Under scenario RCP 8.5, a decrease of e is simulated in the subtropics of Eurasia. This increase is much less visible in change of BA during these two centuries under the same scenario. As a result, this decrease of e is caused by a decrease of the carbon stock in these regions.

In the vast region of boreal Eurasia, in the 22nd–23rd centuries our model simulates both soil drying and overall decrease of the vegetation carbon stock (Fig. 7e–h). As a result, a change of the CO_2 emissions from natural fires in this region is a product of two counteracting effects: an increase of the burnt area due to decreased soil moisture content and a decrease of the vegetation carbon stock. The decreased vegetation carbon stock also leads to smaller relative increase of E_{BOAS} in comparison to that of BA_{BOAS}. In the BONA region, the changes of both these variables are not so pronounced as in Eurasia. This is the reason why relative increases of the burnt area and associated carbon dioxide emissions are smaller than their counterparts in region BOAS.

Similar to those obtained for the 21st century, our results are not very sensitive to specific details of the Bayesian weighting.

4 Caveats

We note some important caveats of our study. They are related to the uncertainties in the GFED-3.1 data, to the uncertainties of our coupled model, and to the assumptions behind the Bayesian averaging.

4.1 Uncertainties in the GFED-3.1 data

First of all, the GFED-3.1 estimates, used to calibrate our model, are uncertain.

The first source of uncertainty arises because the MODIS (MODerate resolution Imaging Spectroradiometer) data, which are used for detection of fires in the GFED algorithm, have a spatial resolution from 500 m to 1 km (van der Werf et al., 2010) and therefore miss the fires with a smaller extent. However, these small fires may contribute very significantly to the burnt area and the respective CO_2 released to the atmosphere (Randerson et al., 2012). The fire identification algorithm is improved in the next-generation GFED data, GFED-4, but the latter data were unavailable at the time of the present paper's preparation. We plan to use the newer data in our future exercises. We note, however, that to date no results have been published concerning the comparison of the simulation results with the data corrected to account for small fires (Randerson et al., 2012).

Another source of uncertainty in the GFED data comes from its usage of the CASA (Carnegie–Ames–Stanford Approach) biogeochemical model to calculate the release of carbon from fires into the atmosphere (van der Werf et al., 2010). As a result, all model uncertainties in simulating vegetation and soil carbon stock propagate to possible uncertainties in fuel stock. However, the CASA model has shown to realistically reproduce carbon fluxes at different temporal scales (Randerson et al., 1997; Angert et al., 2004).

In addition, there is an uncertainty in the values of combustion completeness for different vegetation types and fires

of different origin (van der Werf et al., 2010). To quantify this uncertainty, van der Werf et al. (2010) varied the values of these combustion factors. They reported the respective uncertainty for CO_2 release from fires as large as 20–25 %.

4.2 Caveats related to the coupled model employed

Another source of uncertainty in our work is related to the Earth system model employed (the IAP RAS CM). Its climatology is basically realistic, see Mokhov et al. (2005) for the atmospheric part, Arzhanov et al. (2008) for soil moisture, and Eliseev and Mokhov (2011a) for terrestrial carbon stock. However, as any other climate model, our model exhibits a number of biases, which may affect our simulation of fires.

In particular, the synoptic-scale processes are parametrised in our model (Petoukhov et al., 1998). This leads to the underestimation of weather variability. This is important because fire development depends on climate state in a strongly non-linear fashion. Because our model is only able to reproduce a "smoothed" curve of seasonal changes of the state of the atmosphere and the soil, we could argue that this might affect the results of our calibration. Moreover, such an impact of this parametrisation might be hidden for a present-day climate but affect projections for the 21st–23rd centuries, when climate state is markedly different from the present-day one. In addition, the parametrised synoptic-scale processes lead to the underestimated interannual variability of climate and fire activity. However, the latter is not a major issue for the purpose of this paper, because its focus (together with the presentation of the ensemble approach for simulating natural fires by using the coupled Earth system model) is on climatological means of such characteristics and their sensitivity to climate change. Moreover, our future projections generally agree with the offline simulations reported by Kloster et al. (2012).

Another bias, exhibited by our model, is due to its susceptibility to precipitation increase under warming in most regions (Mokhov et al., 2002), which disagrees with the projections of contemporary general circulation models (e.g. Arblaster et al., 2013). For the historical period, this was partly ameliorated by inclusion of land use impact on the water cycle (Eliseev and Mokhov, 2011b), but the problem still remains for future projections. Acknowledging this important bias of our model, we, however, note that it should lead to the underestimation of future CO_2 released from fires. The work is under way to improve this shortcoming of our model.

We note that these two IAP RAS CM biases, which are presumably the most important for the present work, partly compensate each other.

The fire module implemented in the IAP RAS CM, the GlobFIRM model, is a rather simplistic one. It is known to perform poorly in some small-scale regions (e.g. Thonicke et al., 2001). However, this module is suited well for Earth system models of intermediate complexity because more elaborated natural fire schemes would need an input which
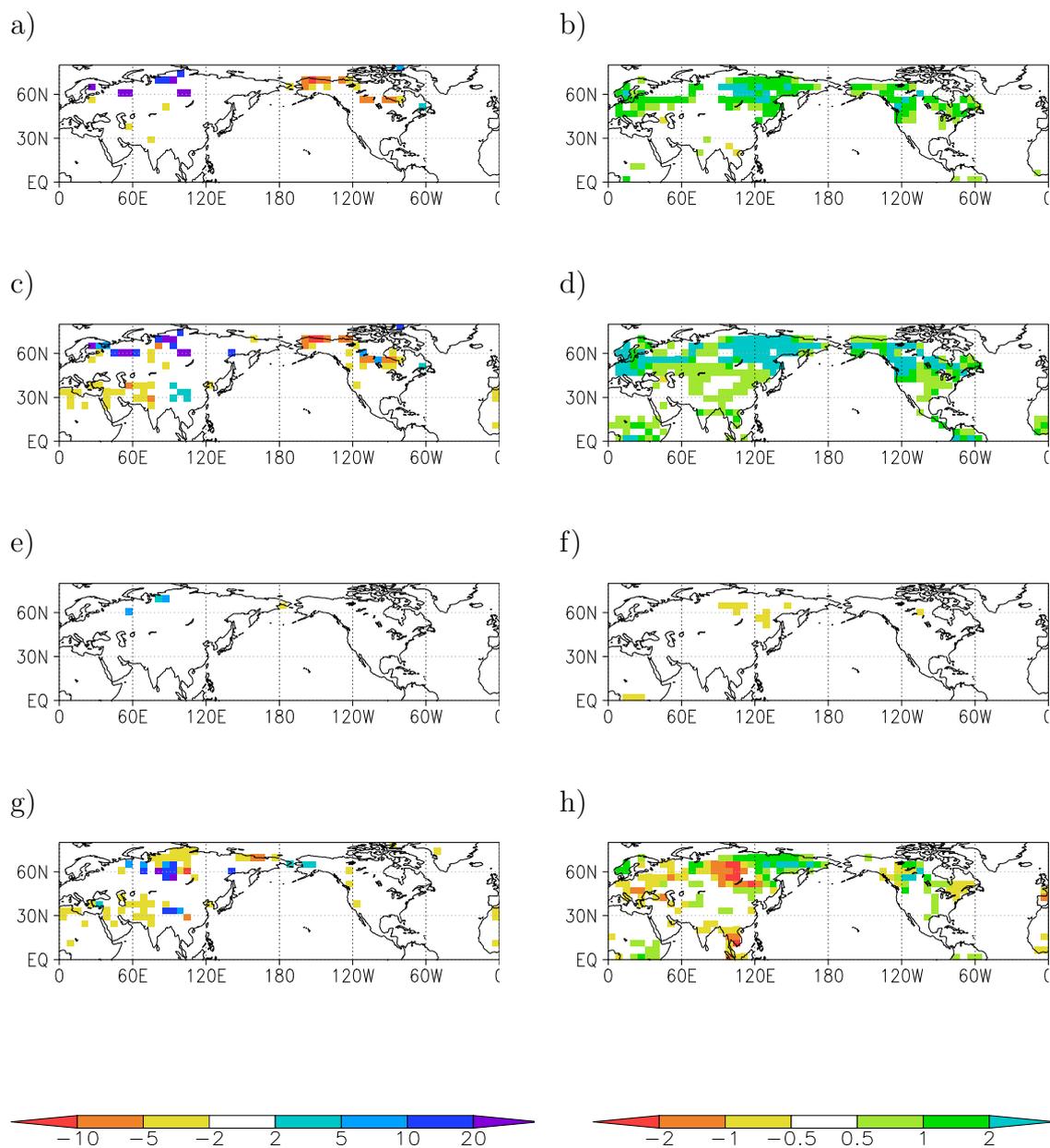
Figure 7. Change of the moisture content of the upper 5 cm of soil (in cm(water) m(soil)$^{-1}$; **a**, **c**, **e**, and **g**) and of the vegetation carbon stock (kg C m^{-2} **b**, **d**, **f**, and **h**) from 1998–2011 to 2091–2100 (**a–d**) and from 2091–2100 to 2291–2300 (**e–h**) for scenarios RCP 2.6 (**a**, **b**, **e**, and **f**) and RCP 8.5 (**c**, **d**, **g**, and **h**).

our model is unable to provide (e.g. the variations of the atmospheric variables at the synoptic scales). In the present paper, the GlobFIRM model was extended by a scheme accounting for the carbon release from soil during fires. The results of the present paper show that this model performs satisfactorily at global and continental scales. Nevertheless, along with an overall development of the IAP RAS CM, we are going to replace it by a more elaborate scheme in the future.

Finally, we have to acknowledge that our calibration is a calibration of the GlobFIRM model within an Earth system model. The latter is reflected, for example, in the values entering Table 2: in many regions realistic CO₂ emissions are obtained for the burnt area which deviates markedly from the GFED data (though not accounting for small fires). Hence, calibration results are likely to differ somewhat if the same GlobFIRM model was forced, e.g. by the reanalysis data. However, the main goal of this paper is a presentation of the ensemble approach to simulate the burnt area and

CO_2 release from natural fires. As a result, all model-related caveats might be considered as tolerable.

We note that our approach may be simplified by dropping the usage of a climate model and applying it only to a land surface scheme incorporating a scheme of natural fires. This would tremendously reduce an involved computational burden. However, it is profitable to model natural fires as a part of the coupled Earth system because, as it was already stated in Sect. 1, the strength of the resulting feedback is not known a priori.

While an assessment of this strength is beyond the scope of the present paper, we made a preliminary attempt to estimate it. In particular, we made two additional runs with our model, one was with the fire scheme is switched on, and another with this scheme is switched off. In the former run, the values of parameters of the fire scheme were set to values calibrated as described in Sect. 3.1. These simulations covered the period 1765–2100 and were forced by the same historical forcings until the year 2005, and by the RCP 8.5 scenario in the period 2006–2100. As expected, we obtained quite a substantial impact on natural fires on vegetation and soil carbon stocks at the regional scale. In particular, natural fires decreased the former by 10–30 % in the fire-prone semiarid regions. The soil carbon stock decrease was the most marked in the Western Siberian Lowlands. In other respects, the feedback between natural fires and the climate state appeared to be modest. In particular, until the first quarter of the 21st century, the difference of the atmospheric CO_2 content in the atmosphere between these two runs was about 1 ppmv (parts per million by volume). It increased to 7 ppmv in the last decade of the 21st century. The resulting instantaneous top-of-the-atmosphere radiative forcing (RF) was smaller than $0.03\,W\,m^{-2}$, and the corresponding difference of the globally averaged surface air temperature between these two runs was always below 0.01 K.

However, we note that Ward et al. (2012) obtained much larger, about $1\,W\,m^{-2}$, fire-induced RF in their offline simulations (an atmospheric general circulation model was forced by the fire emissions archived by the CLM) for time slices corresponding to the years 1850 and 2000. Such radiative forcing is comparable, for example, to the estimated anthropogenic radiative forcing since the preindustrial period to the year 2005 ($0.6 - 2.4\,W\,m^{-2}$ with a central estimate of $1.6\,W\,m^{-2}$, Forster et al., 2007) and might markedly affect the climate state. The precise reasons for this difference between our results and the results by Ward et al. (2012) are unclear. We conclude that a parametric sensitivity of the natural fire–climate feedback deserves further study.

4.3 Caveats related to the averaging procedure

The last caveat we would like to mention is related to the assumptions behind the Bayesian averaging procedure. The latter is based on the assumption which is common for many ensemble-based projections: the members, which are suffi- ciently successful in reproducing available observations, are considered to be the most realistic for future changes as well (Kass and Raftery, 1995; Leroy, 1998; Hoeting et al., 1999; Greene et al., 2006; Kattsov et al., 2007; Khon et al., 2010; Arzhanov et al., 2012). For our model, as well as for other process-based models, this assumption might be heuristically justified by indicating that the processes, which are believed to be most important for the problem at hand, are implemented in the model, and the Bayesian approach is used only to calibrate the parameters of the model. We note that, despite such a drawback, the Bayesian projections are meaningful for future projections of different components of the Earth system (Kass and Raftery, 1995; Leroy, 1998; Hoeting et al., 1999; Greene et al., 2006; Eliseev, 2008, 2011; Arzhanov et al., 2012).

We also note that there is always a lot of subjectivity in the choice of the cost function which is used to calculate weights of individual ensemble members. For instance, our calculation of Bayesian weights lacks any information on interannual fire variability. This is a drawback, but it is consistent with the underestimation of the natural variability by our Earth system model.

In addition, the IAP RAS CM climatology may differ between different ensemble members due to variation of the parameters of the GlobFIRM model. However, this difference is very small. This is true even for the vegetation and soil carbon stocks directly affected by fires.

We stress again that the presentation of the ensemble approach to simulate the burnt area and CO_2 release from natural fires is a main goal of this paper. While this approach is applied here for a simplified Earth system model, it is applicable to ensembles constructed by using more sophisticated models as well (e.g. the CMIP5 ensemble). A systematic application of the Bayesian averaging to the latter ensemble is beyond the scope of this study. Nevertheless, we plan to use it for the latter ensemble in our future work.

5 Conclusions

We performed simulations with the global climate model developed at the A. M. Obukhov Institute of Atmospheric Physics, Russian Academy of Sciences (IAP RAS CM). According to the CMIP5 experimental protocol, the model was forced by the historical reconstruction of external forcings for the period 850–2005 and by the RCP scenarios till the year 2300. In contrast to other studies on a global-scale natural fire activity, our simulations were set up in an ensemble fashion. Different ensemble members were constructed by varying the parameters of the IAP RAS CM module to simulate natural fires. Further, these members are constrained by the GFED-3.1 observational data set and subjected to the Bayesian averaging. In addition, we extended the Glob-FIRM model, implemented in the IAP RAS CM, by a scheme accounting for carbon release from soil during fires. Our

simulations are the first coupled model assessment of future changes in gross characteristics of natural fires.

In our simulations, the present-day (1998–2011) global area burnt due to natural fires is $(2.1 \pm 0.4) \times 10^6 \, \text{km}^2 \, \text{yr}^{-1}$ (the ensemble means and intra-ensemble standard deviations are presented), and the respective CO_2 emissions to the atmosphere are $(1.4 \pm 0.2) \, \text{Pg C} \, \text{yr}^{-1}$. The latter value is in agreement with the corresponding observational estimates. Regionally, the modelled CO_2 emissions are smaller than the GFED estimates in the tropics; in the extratropics, the simulated emissions are smaller (larger) than these estimates in north-eastern Eurasia (in Europe).

Our model simulates a drastic increase of the burnt area and the respective carbon dioxide emissions provided that anthropogenic forcing continues to grow in the next few centuries. From 1998–2011 to 2091–2100, the ensemble mean global burnt area increased by 13 % (28 %, 36 %, 51 %) under scenario RCP 2.6 (RCP 4.5, RCP 6.0, RCP 8.5). The corresponding global emissions increase is 14 % (29 %, 37 %, 42 %). From 2091–2100 to 2291–2300, under the mitigation scenario RCP 2.6 the ensemble mean global burnt area and respective CO_2 emissions slightly decrease, both by 5 % relative to their values in the period 2091–2100. In turn, under scenario RCP 4.5 (RCP 6.0, RCP 8.5) the ensemble mean burnt area in the period 2291–2100 is higher by 15 % (44 %, 83 %) than its value in years 2091–2100, and the ensemble mean CO_2 emissions are correspondingly higher by 9 % (19 %, 31 %). The simulated changes of natural fire characteristics in the 21st–23rd centuries are associated mostly with the corresponding changes in the boreal regions of Eurasia and North America. In particular, in boreal Eurasia and North America, an increase of both the ensemble mean burnt area and CO_2 emissions due to natural fires may be several times larger. Under the RCP 8.5 scenario, an increase of the burnt area and CO_2 emissions in boreal regions during the 22nd and 23rd centuries, however, is accompanied by the respective decrease in the tropics and subtropics.

Finally, we note that an enhancement of the carbon dioxide release in the atmosphere due to natural fires in the 21st–23rd centuries occurs under strong anthropogenic CO_2 emissions. For instance, an increase of E_g in the 21st century under the RCP 4.5 scenario by $0.2 \, \text{Pg C} \, \text{yr}^{-1}$ is just 5 % of the fossil fuel+industrial carbon dioxide emissions which in this century reach $8 \, \text{Pg C} \, \text{yr}^{-1}$ under this scenario. An even smaller respective percentage is found for scenarios RCP 6.0 and RCP 8.5. As a result, an enhancement of e in the next several centuries under the RCP scenarios does not affect the atmospheric carbon dioxide content. The latter may be used in the process of the development of international agreements similar to the Kyoto Protocol.

The Supplement related to this article is available online at doi:10.5194/bg-11-3205-2014-supplement.

References

Andreae, M. and Merlet, P.: Emission of trace gases and aerosols from biomass burning, Glob. Biogeochem. Cy., 15, 955–966, doi:10.1029/2000GB001382, 2001.

Angert, A., Biraud, S., Bonfils, C., and Fung, I.: CO_2 seasonality indicates origins of post–Pinatubo sink, Geophys. Res. Lett., 31, L11103, doi:10.1029/2004GL019760, 2004.

Arblaster, J., Dufresne, J.-L., Fichefet, T., Friedlingstein, P., Gao, X., Gutowski, W., Johns, T., Krinner, G., Shongwe, M., Tebaldi, C., Weaver, A., and Wehner, M.: Long–term climate change: Projections, commitments and irreversibility, in: Climate Change 2013: The Physical Science Basis. Contribution of Working Group I to the Fifth Assessment Report of the Intergovernmental Panel on Climate Change, edited by: Stocker, T., Qin, D., Plattner, G.-K., Tignor, M., Allen, S., Boschung, J., Nauels, A., Xia, Y., Bex, V., and Midgley, P., 1029–1136, Cambridge University Press, Cambridge and New York, 2013.

Arora, V. and Boer, G.: Fire as an interactive component of dynamic vegetation models, J. Geophys. Res., 110, G02008, doi:10.1029/2005JG000042, 2005.

Arzhanov, M., Demchenko, P., Eliseev, A., and Mokhov, I.: Simulation of characteristics of thermal and hydrologic soil regimes in equilibrium numerical experiments with a climate model of intermediate complexity, Izvestiya, Atmos. Ocean. Phys., 44, 279–287, doi:10.1134/S0001433808050022, 2008.

Arzhanov, M., Eliseev, A., and Mokhov, I.: A global climate model based, Bayesian climate projection for northern extra–tropical land areas, Glob. Planet. Change, 86–87, 57–65, doi:10.1016/j.gloplacha.2012.02.001, 2012.

Ciais, P., Sabine, C., Bala, G., Bopp, L., Brovkin, V., Canadell, J., Chhabra, A., DeFries, R., Galloway, J., Heimann, M., Jones, C., Le Quéré, C., Myneni, R., Piao, S., and Thornton, P.: Carbon and other biogeochemical cycles, in: Climate Change 2013: The Physical Science Basis. Contribution of Working Group I to the Fifth Assessment Report of the Intergovernmental Panel on Climate Change, edited by: Stocker, T., Qin, D., Plattner, G.-K., Tignor, M., Allen, S., Boschung, J., Nauels, A., Xia, Y., Bex, V., and Midgley, P., 465–570, Cambridge University Press, Cambridge and New York, 2013.

Claussen, M., Mysak, L., Weaver, A., Crucifix, M., Fichefet, T., Loutre, M.-F., Weber, S., Alcamo, J., Alexeev, V., Berger, A., Calov, R., Ganopolski, A., Goosse, H., Lohmann, G., Lunkeit, F., Mokhov, I., Petoukhov, V., Stone, P., and Wang, Z.: Earth system models of intermediate complexity: closing the gap in the

spectrum of climate system models, Clim. Dynam., 18, 579–586, doi:10.1007/s00382-001-0200-1, 2002.

Conard, S., Sukhinin, A., Stocks, B., Cahoon, D., Davidenko, E., and Ivanova, G.: Determistic effects of area burned and fire severity on carbon cycling and emissions in Siberia, Clim. Change, 55, 197–211, doi:10.1023/A:1020207710195, 2002.

Crutzen, P., Delany, A., Greenberg, J., Haagenson, P., Heidt, L., Lueb, R., Pollock, W., Seiler, W., Wartburg, A., and Zimmerman, P.: Tropospheric chemical composition measurements in Brazil during the dry season, J. Atmos. Chem., 2, 233–256, doi:10.1007/BF00051075, 1985.

Eby, M., Weaver, A. J., Alexander, K., Zickfeld, K., Abe-Ouchi, A., Cimatoribus, A. A., Crespin, E., Drijfhout, S. S., Edwards, N. R., Eliseev, A. V., Feulner, G., Fichefet, T., Forest, C. E., Goosse, H., Holden, P. B., Joos, F., Kawamiya, M., Kicklighter, D., Kienert, H., Matsumoto, K., Mokhov, I. I., Monier, E., Olsen, S. M., Pedersen, J. O. P., Perrette, M., Philippon-Berthier, G., Ridgwell, A., Schlosser, A., Schneider von Deimling, T., Shaffer, G., Smith, R. S., Spahni, R., Sokolov, A. P., Steinacher, M., Tachiiri, K., Tokos, K., Yoshimori, M., Zeng, N., and Zhao, F.: Historical and idealized climate model experiments: an intercomparison of Earth system models of intermediate complexity, Clim. Past, 9, 1111–1140, doi:10.5194/cp-9-1111-2013, 2013.

Elansky, N., Mokhov, I., Belikov, I., Berezina, E., Elokhov, A., Ivanov, V., Pankratova, N., Postylyakov, O., Safronov, A., Skorokhod, A., and Shumskii, R.: Gaseous admixtures in the atmosphere over Moscow during the 2010 summer, Izvestiya, Atmos. Ocean. Phys., 47, 672–681, doi:10.1134/S000143381106003X, 2011.

Eliseev, A.: Estimation of the uncertainty of future changes in atmospheric carbon dioxide concentration and its radiative forcing, Izvestiya, Atmos. Ocean. Phys., 44, 279–287, doi:10.1134/S0001433808030031, 2008.

Eliseev, A.: Estimation of changes in characteristics of the climate and carbon cycle in the 21st century accounting for the uncertainty of terrestrial biota parameter values, Izvestiya, Atmos. Ocean. Phys., 47, 131–153, doi:10.1134/S0001433811020046, 2011.

Eliseev, A.: Climate change mitigation via sulfate injection to the stratosphere: impact on the global carbon cycle and terrestrial biosphere, Atmos. Ocean. Optics, 25, 405–413, doi:10.1134/S1024856012060024, 2012.

Eliseev, A. and Mokhov, I.: Uncertainty of climate response to natural and anthropogenic forcings due to different land use scenarios, Adv. Atmos. Sci., 28, 1215–1232, doi:10.1007/s00376-010-0054-8, 2011a.

Eliseev, A. and Mokhov, I.: Effect of including land use driven radiative forcing of the surface albedo of land on climate response in the 16th–21st centuries, Izvestiya, Atmos. Ocean. Phys., 47, 15–30, doi:10.1134/S0001433811010075, 2011b.

Eliseev, A. and Sergeev, D.: Impact of subgrid–scale heterogeneity of vegetation on the results of simulation of carbon cycle characteristics, Izvestiya, Atmos Ocean Phys., 50, 225–235, doi:10.1134/S0001433814020030, 2014.

Eliseev, A., Coumou, D., Chernokulsky, A., Petoukhov, V., and Petri, S.: Scheme for calculation of multi–layer cloudiness and precipitation for climate models of intermediate complexity, Geosci. Model. Dev., 6, 1745–1765, doi:10.5194/gmd-6-1745-2013, 2013.

Forster, P., Ramaswamy, V., Artaxo, P., Berntsen, T., Betts, R., Fahey, D., Haywood, J., Lean, J., Lowe, D., Myhre, G., Nganga, J., R. Prinn, J., Raga, G., Schulz, M., and Van Dorland, R.: Changes in atmospheric constituents and in radiative forcing, in: Climate Change 2007: The Physical Science Basis, edited by: Solomon, S., Qin, D., Manning, M., Marquis, M., Averyt, K., Tignor, M., LeRoy Miller, H., and Chen, Z., 129–234, Cambridge University Press, Cambridge/New York, 2007.

Greene, A., Goddard, L., and Lall, U.: Probabilistic multimodel regional temperature change projections, J. Climate, 19, 4326–4343, doi:10.1175/JCLI3864.1, 2006.

Hoeting, J., Madigan, D., Raftery, A., and Volinsky, C.: Bayesian model averaging: A tutorial, Stat. Sci., 14, 382–401, 1999.

Hughes, R., Kauffman, J., and Cummings, D.: Fire in the Brazilian Amazon: 3. Dynamics of biomass, C, and nutrient pools in regenerating forests, Oecologia, 124, 574–588, 2000.

Kass, R. and Raftery, A.: Bayes factors, J. Amer. Stat. Assoc., 90, 773–795, 1995.

Kattsov, V., Walsh, J., Chapman, W., Govorkova, V., Pavlova, T., and Zhang, X.: Simulation and projection of Arctic freshwater budget components by the IPCC AR4 global climate models, J. Hydrometeorol., 8, 571–589, doi:10.1175/JHM575.1, 2007.

Khon, V., Mokhov, I., Latif, M., Semenov, V., and Park, W.: Perspectives of Northern Sea Route and Northwest Passage in the twenty–first century, Clim. Change, 100, 757–768, doi:10.1007/s10584-009-9683-2, 2010.

Kloster, S., Mahowald, N., Randerson, J., Thornton, P., Hoffman, F., Levis, S., Lawrence, P., Feddema, J., Oleson, K., and Lawrence, D.: Fire dynamics during the 20th century simulated by the Community Land Model, Biogeosciences, 7, 1877–1902, doi:10.5194/bg-7-1877-2010, 2010.

Kloster, S., Mahowald, N., Randerson, J., and Lawrence, P.: The impacts of climate, land use, and demography on fires during the 21st century simulated by CLM–CN, Biogeosciences, 9, 509–525, doi:10.5194/bg-9-509-2012, 2012.

Konovalov, I., Beekmann, M., Kuznetsova, I., Yurova, A., and Zvyagintsev, A.: Atmospheric impacts of the 2010 Russian wildfires: integrating modelling and measurements of an extreme air pollution episode in the Moscow region, Atmos. Chem. Phys., 11, 10031–10056, doi:10.5194/acp-11-10031-2011, 2011.

Leroy, S.: Detecting climate signals: Some Bayesian aspects, J. Climate, 11, 640–651, 1998.

Li, F., Zeng, X., and Levis, S.: A process–based fire parameterization of intermediate complexity in a Dynamic Global Vegetation Model, Biogeosciences, 9, 2761–2780, doi:10.5194/bg-9-2761-2012, 2012.

Li, F., Levis, S., and Ward, D.: Quantifying the role of fire in the Earth system — Part 1: Improved global fire modeling in the Community Earth System Model (CESM1), Biogeosciences, 10, 2293–2314, doi:10.5194/bg-10-2293-2013, 2013.

Mack, M., Bret-Harte, M., Hollingsworth, T., Jandt, R., Schuur, E., Shaver, G., and Verbyla, D.: Carbon loss from an unprecedented Arctic tundra wildfire, Nature, 475, 289–492, doi:10.1038/nature10283, 2011.

McKay, M., Beckman, R., and Conover, W.: A comparison of three methods for selecting values of input variables in the analysis of output from a computer code, Technometrics, 21, 239–245, 1979.

Mokhov, I. and Chernokulsky, A.: Regional model assessments of forest fire risks in the Asian part of Russia under climate change, Geogr. Nat. Resour., 31, 165–169, doi:10.1016/j.gnr.2010.06.012, 2010.

Mokhov, I. and Eliseev, A.: Modeling of global climate variations in the 20th–23rd centuries with new RCP scenarios of anthropogenic forcing, Doklady Earth Sci., 443, 532–536, doi:10.1134/S1028334X12040228, 2012.

Mokhov, I., Demchenko, P., Eliseev, A., Khon, V., and Khvorostyanov, D.: Estimation of global and regional climate changes during the 19th–21st centuries on the basis of the IAP RAS model with consideration for anthropogenic forcing, Izvestiya, Atmos. Ocean. Phys., 38, 555–568, 2002.

Mokhov, I., Eliseev, A., Demchenko, P., Khon, V., Akperov, M., Arzhanov, M., Karpenko, A., Tikhonov, V., Chernokulsky, A., and Sigaeva, E.: Climate changes and their assessment based on the IAP RAS global model simulations, Doklady Earth Sci., 402, 591–595, 2005.

Moss, R., Edmonds, J., Hibbard, K., Manning, M., Rose, S., van Vuuren, D., Carter, T., Emori, S., Kainuma, M., Kram, T., Meehl, G., Mitchell, J., Nakicenovic, N., Riahi, K., Smith, S., Stouffer, R., Thomson, A., Weyant, J., and Wilbanks, T.: The next generation of scenarios for climate change research and assessment, Nature, 463, 747–756, doi:10.1038/nature08823, 2010.

Nakićenović, N., Alcamo, J., Davis, G., de Vries, B., Fenhann, J., Gaffin, S., Gregory, K., Grübler, A., Jung, T., Kram, K., La Rovere, L., Michaelis, L., Mori, S., Morita, T., Pepper, W., Pitcher, H., Price, L., Raihi, K., Roehrl, A., Rogner, H.-H., Sankovski, A., Schlesinger, M., Shukla, P., Smith, S., Swart, R., van Rooijen, S., Victor, N., and Dadi, Z.: IPCC Special Report on Emission Scenarios, Cambridge University Press, New York, 2000.

Petoukhov, V., Mokhov, I., Eliseev, A., and Semenov, V.: The IAP RAS Global Climate Model, Dialogue–MSU, Moscow, 1998.

Petoukhov, V., Claussen, M., Berger, A., Crucifix, M., Eby, M., Eliseev, A., Fichefet, T., Ganopolski, A., Goosse, H., Kamenkovich, I., Mokhov, I., Montoya, M., Mysak, L., Sokolov, A., Stone, P., Wang, Z., and Weaver, A.: EMIC intercomparison project (EMIP–CO2): Comparative analysis of EMIC simulations of current climate and equilibrium and transient responses to atmospheric CO$_2$ doubling, Clim. Dynam., 25, 363–385, doi:10.1007/s00382-005-0042-3, 2005.

Randerson, J., Thompson, M., Conway, M., Fung, I., and Field, C.: The contribution of terrestrial sources and sinks to trends in the seasonal cycle of atmospheric carbon dioxide, Glob. Biogeochem. Cy., 11, 535–560, doi:10.1029/97GB02268, 1997.

Randerson, J., Chen, Y., van der Werf, G., Rogers, B., and Morton, D.: Global burned area and biomass burning emissions from small fires, J. Geophys. Res.-Biogeo., 117, G04012, doi:10.1029/2012JG002128, 2012.

Sheng, Y., Smith, L., MacDonald, G., Kremenetski, K., Frey, K., Velichko, A., Lee, M., Beilman, D., and Dubinin, P.: A high-resolution GIS–based inventory of the west Siberian peat carbon pool, Glob. Biogeochem. Cy., 18, GB3004, doi:10.1029/2003GB002190, 2004.

Sitch, S., Smith, B., Prentice, I., Arneth, A., Bondeau, A., Cramer, W., Kaplan, J., Levis, S., Lucht, W., Sykes, M., Thonicke, K., and Venevsky, S.: Evaluation of ecosystem dynamics, plant geography and terrestrial carbon cycling in the LPJ dynamic global vegetation model, Glob. Change Biol., 9, 161–185, doi:10.1046/j.1365-2486.2003.00569.x, 2003.

Stein, M.: Large sample properties of simulations using latin hypercube sampling, Technometrics, 29, 141–150, doi:10.2307/1269769, 1987.

Taylor, K.: Summarizing multiple aspects of model performance in a single diagram, J. Geophys. Res., 106, 7183–7192, doi:10.1029/2000JD900719, 2001.

Taylor, K., Stouffer, R., and Meehl, G.: An overview of CMIP5 and the experiment design, B. Am. Meteorol. Soc., 93, 485–498, doi:10.1175/BAMS-D-11-00094.1, 2012.

Thonicke, K., Venevsky, S., Sitch, S., and Cramer, W.: The role of fire disturbance for global vegetation dynamics: coupling fire into a Dynamic Global Vegetaion Model, Glob. Ecol. Biogeogr., 10, 661–677, 2001.

Thonicke, K., Spessa, A., Prentice, I., Harrison, S., Dong, L., and Carmona-Moreno, C.: The influence of vegetation, fire spread and fire behaviour on biomass burning and trace gas emissions: results from a process–based model, Biogeosciences, 7, 1991–2011, doi:10.5194/bg-7-1991-2010, 2010.

Tucker, C., Pinzon, J., Brown, M., Slayback, D., Pak, E., and Mahoney, R.: An extended AVHRR 8-km NDVI data set compatible with MODIS and SPOT vegetation NDVI data, Int. J. Remote Sens., 26, doi:10.1080/01431160500168686, 2005.

Turquety, S., Menut, L., Bessagnet, B., Anav, A., Viovy, N., Maignan, F., and Wooster, M.: APIFLAME v1.0: high-resolution fire emission model and application to the Euro-Mediterranean region, Geosci. Model. Dev., 7, 587–612, doi:10.5194/gmd-7-587-2014, 2014.

van der Werf, G., Randerson, J., Giglio, L., Collatz, G., Mu, M., Kasibhatla, P. S., Morton, D., DeFries, R., Jin, Y., , and van Leeuwen, T.: Global fire emissions and the contribution of deforestation, savanna, forest, agricultural, and peat fires (1997–2009), Atmos. Chem. Phys., 10, 11707–11735, doi:10.5194/acp-10-11707-2010, 2010.

Ward, D., Kloster, S., Mahowald, N., Rogers, B., Randerson, J., and Hess, P.: The changing radiative forcing of fires: global model estimates for past, present and future, Atmos. Chem. Phys., 12, 10857–10886, doi:10.5194/acp-12-10857-2012, 2012.

Zickfeld, K., Eby, M., Weaver, A., Alexander, K., Crespin, E., Edwards, N., Eliseev, A., Feulner, G., Fichefet, T., Forest, C., Friedlingstein, P., Goosse, H., Holden, P., Joos, F., Kawamiya, M., Kicklighter, D., Kienert, H., Matsumoto, K., Mokhov, I., Monier, E., Olsen, S., Pedersen, J., Perrette, M., Philippon-Berthier, G., Ridgwell, A., Schlosser, A., Schneider von Deimling, T., Shaffer, G., Sokolov, A., Spahni, R., Steinacher, M., Tachiiri, K., Tokos, K., Yoshimori, M., Zeng, N., and Zhao, F.: Long-term climate change commitment and reversibility: An EMIC intercomparison, J. Climate, 26, 5782–5809, doi:10.1175/JCLI-D-12-00584.1, 2013.